



A Vacuum Ultraviolet Photoionization Study on the Formation of *N*-methyl Formamide (HCONHCH₃) in Deep Space: A Potential Interstellar Molecule with a Peptide Bond

Robert Frigge^{1,2}, Cheng Zhu^{1,2}, Andrew M. Turner^{1,2}, Matthew J. Abplanalp^{1,2}, Alexandre Bergantini^{1,2} , Bing-Jian Sun³, Yue-Lin Chen³, Agnes H. H. Chang³, and Ralf I. Kaiser^{1,2} 

¹ W. M. Keck Research Laboratory in Astrochemistry, University of Hawaii at Manoa, Honolulu, Hawaii 96822, USA; ralfk@hawaii.edu

² Department of Chemistry, University of Hawaii at Manoa, Honolulu, Hawaii 96822, USA

³ Department of Chemistry, National Dong Hwa University, Shoufeng, Hualien 974, Taiwan

Received 2018 April 6; revised 2018 June 4; accepted 2018 June 8; published 2018 July 25

Abstract

As one of the simplest molecules containing a peptide bond, *N*-methyl formamide (HCONHCH₃) represents a potential key molecule involved in the peptide bond polymerization in extraterrestrial ices. Detected tentatively toward the star-forming region Sgr B2(N2), the synthetic pathways have previously been elusive. By exploiting isomer-selective detection of the reaction products via photoionization, coupled with reflectron time-of-flight mass spectrometry (PI-ReTOF-MS), we present compelling evidence for the formation of *N*-methyl formamide (HCONHCH₃) in astrochemically relevant ice mixtures of methylamine (CH₃NH₂) and carbon monoxide (CO), upon irradiation with energetic electrons as generated in the track of galactic cosmic ray particles (GCRs) penetrating interstellar ices. As one of the simplest molecules containing a peptide bond (–CO–NH–), *N*-methyl formamide could represent a benchmark involved in radiation-induced peptide bond polymerization in extraterrestrial ices, and thus bring us closer to revealing where in the Universe the molecular precursors linked to the origins of life might have been synthesized.

Key words: astrobiology – astrochemistry – cosmic rays – ISM: molecules – methods: laboratory: solid state – molecular processes

1. Introduction

In recent decades, the origin of the peptide bond (–CO–NH–) in extraterrestrial environments has received considerable attention from both the astrochemistry and astrobiology communities (Ehrenfreund & Chamley 2000; Ehrenfreund et al. 2012). The possibilities suggested by peptide polymerization via amino acid recombination represents one of the fundamental concepts for all life on Earth (Kaiser et al. 2013). Formamide (HCONH₂) as observed toward SGR B2 (Rubin et al. 1971; Gottlieb et al. 1973) represents the simplest molecule carrying the amide (peptide) moiety and can be synthesized along with urea (CO(NH₂)₂) (Förstel et al. 2016a) via barrier-less radical–radical recombination throughout astrophysically relevant carbon monoxide (CO)–ammonia (NH₃) ices exposed to energetic electrons at 10 K (Jones et al. 2011). The recent tentative detection of *N*-methyl formamide (HCONHCH₃) toward Sgr B2(N2) (Belloche et al. 2017) represents a significant step toward advancing interstellar prebiotic chemistry (Kaiser et al. 2013), due to the methyl-substituted peptide bond present in this molecule. As a catalyst, *N*-methyl formamide could also play a role in the predisposition of chirality in organic molecules in the interstellar medium. Malkov et al. (2006) analyzed multiple organic catalysts involved in the ketamine transformation to secondary amines, revealing *N*-methyl formamide (HCONHCH₃), combined with anilide (C₆H₅NH–R), as a promising candidate to form secondary amines that are enantiomer selective in the presence of the *N*-methyl group.

However, despite the importance of *N*-methyl formamide (HCONHCH₃) as a potential building block to polyamides in deep space, the underlying formation routes have not yet been unraveled. Ligterink et al. (2017) revealed that the chemically related methyl isocyanate (CH₃NCO) molecule is synthesized in low-temperature (12 K) isocyanic acid (HNCO)–methane

(CH₄) ices exposed to vacuum ultraviolet (VUV) radiation at 121 nm and in the range of 140 to 160 nm. However, *N*-methyl formamide (HCONHCH₃), formally a hydrogenation product of methyl isocyanate (CH₃NCO), could not be probed. Bossa et al. (2012) photolyzed methylamine (CH₃NH₂) and carbon monoxide (CO) ices at 20 K and detected an ion signal via a quadrupole mass spectrometer (QMS) at $m/z = 59$ (C₂H₅NO⁺ after electron impact ionization of the subliming molecules. In their photolysis study they found small features in their FTIR study around 1722 cm^{–1} and 1683 cm^{–1}, which they postulated to originate from amides or aldehydes. Therefore, they related the $m/z = 59$ during sublimation in the QMS to *N*-methyl formamide. In their experiment they used UV flux of 10¹⁵ photons s^{–1} cm^{–2}. However, since electron impact ionization does not present an isomer-selective ionization tool, (Kaiser et al. 2015; Abplanalp et al. 2016a; Förstel et al. 2016b; Tarczay et al. 2016) the authors defined this ion signal as a possible link to *N*-methyl formamide. These considerations reveal that the elucidation of the synthetic pathway to *N*-methyl formamide in low-temperature interstellar analog ices exposed to ionizing radiation is still in its infancy.

Here, we exploit single photon ionization (PI), coupled with a reflection time-of-flight mass spectrometer (ReTOF-MS), to ionize and to detect *N*-methyl formamide isomer selectively. PI-ReTOF-MS represents a unique approach in space simulation chambers to selectively ionize distinct structural isomers based on their ionization energies once they have sublimed into the gas phase in the temperature-programmed desorption phase (TPD) after exposing astrophysical model ices to ionizing radiation. If the photon energy is close to the ionization threshold, insignificant internal energy can be channeled into the ion, and ideally fragmentation of the parent molecular ion can be avoided (Abplanalp et al. 2016a). Likewise, employing distinct photon energies of 10.82 eV and 9.78 eV, all CH₃NO

isomers can be ionized at 10.82 eV, whereas at 9.78 eV all isomers *except* *N*-methyl formamide (HCONHCH₃) are ionized. Combined with isotopic substitution studies, which trace the isotopic shift of *N*-methyl formamide via the m/z values, the present study demonstrates for the first time unambiguously that *N*-methyl formamide can be synthesized in low-temperature (5 K) interstellar model ices of methylamine (CH₃NH₂) and carbon monoxide (CO) exposed to ionizing radiation in the form of energetic electrons mimicking secondary electrons released during the passage of galactic cosmic rays (GCR) through interstellar ices (Bennett et al. 2007). While carbon monoxide has already been detected in interstellar ices with an abundance to water of about 20% (Reach et al. 2013), up to now, methylamine has only been detected in the gas phase in the interstellar medium (Fourikis et al. 1974). However, compelling evidence can be found that its formation also took place in interstellar ices via recombination of methyl (CH₃) and amidogen (NH₂) radicals (Förstel et al. 2017). Methane (CH₄) and ammonia (NH₃) have been detected in interstellar ices by the infrared space observatory (Gürtler et al. 2002). Their respective abundances relative to water are typically 1% and 5%, respectively (Boogert et al. 1996, 1997; Gürtler et al. 2002). Neighboring molecules of methane (CH₄) and ammonia (NH₃) in interstellar ice mixtures can undergo C-H and N-H bond rupture to methyl and amidogen radicals and thus can recombine to methylamine upon radiation (Holtom et al. 2005; Förstel et al. 2017). Therefore, the present laboratory simulation experiments mirror the exposure of carbon monoxide and methylamine in interstellar ices in cold molecular clouds by GCR's over the lifetime of the cloud of typically 10⁷ years (Moore et al. 2001), followed by their transition to star-forming regions and ice sublimation as simulated via the TPD phase. Considering that molecular clouds constitute the nurseries of stars and planetary systems, (Garrod et al. 2008; Herbst & van Dishoeck 2009; Walsh et al. 2014), the identification of *N*-methyl formamide proposes that this molecule can be partially incorporated into solar system bodies such as comets, thus opening the door for prospective searches for this key tracer in our solar system.

2. Experimental Details

The experiments were performed at the W. M. Keck Research Laboratory in Astrochemistry (Abplanalp et al. 2016a). The experimental setup consists of a steel ultra high vacuum chamber (UHV) operated at a base pressure of a few 10⁻¹¹ Torr. A polished silver wafer located within the chamber is coupled to a cold finger cooled to 5.5 ± 0.1 K using a UHV compatible closed-cycle helium compressor (Sumitomo Heavy Industries, RDK-415E). The target can be translated in the vertical axis and rotated in the horizontal plane. A gas mixture of methylamine (CH₃NH₂, Sigma Aldrich; 99.9999%) and carbon monoxide (CO, Matheson TriGas, 99.999%) prepared in a gas mixing chamber at a ratio of 1:3.5 was deposited onto the cooled silver wafer *via* a glass capillary at a base pressure of 5.5 × 10⁻⁸ Torr for 20 minutes until the desired ice thickness was achieved. This ice growth was monitored online and in situ via an interference pattern of the HeNe laser (λ = 632.8 nm; CVI Melles-Griot; 25-LHP-230) reflected from the silver wafer and the ice surface. The recorded fringes translate into an ice thickness via Equation (1), which defines the thickness (d) of an ice and the dependence on the number of interference

Table 1
Data Applied to Calculate the Irradiation Dose per Molecule

initial kinetic energy of the electrons, E_{init}	5 keV
irradiation current, I	50 ± 2 nA
total number of electrons	(1.12 ± 0.3) × 10 ¹⁵
average kinetic energy of backscattered electrons, E_{bs} ^a	3.25 ± 0.3 keV
fraction of backscattered electrons, f_{bs} ^a	0.4 ± 0.1
average kinetic energy of transmitted electrons, E_{trans} ^a	2.9 ± 0.3 keV
fraction of transmitted electrons, f_{trans} ^a	0
average penetration depth, l^a	235 ± 80 nm
density of the ice, ρ	1.2 ± 0.1 g cm ⁻³
irradiated area, A	1.0 ± 0.1 cm ²
total number of molecules processed ^b	(5 ± 1) × 10 ¹⁷
dose per CH ₃ NH ₂ , D^b	11 ± 1 eV
dose per CO, D^b	10 ± 1 eV

Notes.

^a Values from CASINO Simulations.

^b Derived values based on 50 nA, 60-minute irradiation of ice mixtures containing methylamine(CH₃NH₂) and carbon monoxide (CO).

fringes (m), the laser wavelength (λ), and the angle of incidence of the laser beam ($\theta = 4^\circ$): (Turner et al. 2015; Förstel et al. 2016b, 2016c; Tsegaw et al. 2017)

$$d = \frac{m\lambda}{2\sqrt{n^2 - \sin^2\theta}}. \quad (1)$$

With the weighted average refractive index (n) for methylamine (CH₃NH₂) ice of 1.40 ± 0.3 and carbon monoxide (CO) ice of 1.25 ± 0.03, (Bouilloud et al. 2015) a thickness of 550 ± 50 nm is determined. This is confirmed by the calculation of the thickness via the infrared absorption strength A_{ex} and the peak area $\int A_{\text{peak}}(\nu) d\nu$ via Equation (2), where M is the molecular weight, N_A is Avogadro's number, and α is the angle of the incoming beam inside of the ice: (Turner et al. 2015)

$$d = \frac{\ln(10)M \int A_{\text{peak}}(\nu) d\nu}{2N_A \rho n A_{\text{ex}}} \sqrt{n^2 - \sin^2\alpha}. \quad (2)$$

For methylamine (CH₃NH₂) the absorption strength of 1.0 ± 0.2 × 10⁻¹⁸ cm molecule⁻¹ at 2750 cm⁻¹ (ν_3) is derived experimentally from a pure methylamine ice with a known thickness and results in 170 ± 50 nm. The absorption strength of 1.3 ± 0.1 × 10⁻¹⁷ at 2139 cm⁻¹ of carbon monoxide (CO) is taken from Bouilloud et al. (2015), which results in a thickness of 320 ± 50 nm. Given the densities of 0.85 g cm⁻³ (Holtom et al. 2007) for methylamine (CH₃NH₂) and 0.80 g cm⁻³ (Bouilloud et al. 2015) for carbon monoxide (CO), the overall thickness results in 510 ± 100 nm. Based on the absorptions in the infrared spectrum, the ratio of methylamine (CH₃NH₂) to carbon monoxide (CO) is 1:2 ± 0.5 within the ice. After the deposition, an area of 1.0 ± 0.1 cm² of the ice mixture was irradiated with 5 keV electrons for 60 minutes, with an electron current of 50 nA at an angle of incidence of 70° relative to the surface normal. This corresponds to a flux of 9.4 × 10¹¹ electrons per second. Galactic cosmic rays interacting with interstellar ices consist mainly of protons with kinetic energies of up to PeV. An interaction of these GCRs with solids generates a cascade of secondary electrons with energies in the range from a

Table 2
Parameter for the Vacuum Ultraviolet Light Generation Used in the Present Experiments

	Photoionization energy/eV	10.82	9.78
	Flux (10^{11} photons s^{-1})	$(6 \pm 1) \times 10^{11}$	$(7 \pm 1) \times 10^{11}$
$(2\omega_1 - \omega_2)$	Wavelength/nm	114.6	126.8
ω_1	Wavelength/nm	202.316	202.316
Nd:YAG (ω_1)	Wavelength/nm	532	532
Dye laser (ω_1)	Wavelength/nm–dye laser	606.948	606.948
Dye		Rh 610/Rh 640	Rh 610/Rh 640
ω_2	Wavelength/nm	863	500
Nd:YAG (ω_1)	Wavelength/nm–Nd:YAG	532	355
Dye laser (ω_1)	Wavelength/nm–dye laser	863	500
Dye		LDS 867	C503
	Nonlinear medium	Kr	Kr

few eV up to keV (Jones et al. 2011; Abplanalp et al. 2016b; Turner et al. 2016). Therefore, the 5 keV electrons mimic efficiently the irradiation by GCR-induced electron cascades. The thickness, as well as the ratio in this ice, which are far away from interstellar conditions, are used in order to avoid interaction of the electrons with the silver mirror and to increase the reaction between the two compounds. However, the results are transferable. By utilizing CASINO 2.42 software (Drouin et al. 2007) an average penetration depth of 235 ± 80 nm is calculated (Table 1). The average dose absorbed is determined to be 11 ± 1 eV molecule $^{-1}$ and 10 ± 1 eV molecule $^{-1}$ for methyamine and carbon monoxide, respectively. During the irradiation the chemical evolution of the ice mixture was monitored online and in situ using FTIR (Nicolet 6700, MCT-A) in the range of 4500 cm^{-1} – 500 cm^{-1} , with a resolution of 4 cm^{-1} , at a reflection angle of 45° for the absorption-reflection-absorption mode. Once the irradiation was complete, the ice was held isothermally at 5.5 K for an additional 30 minutes before starting TPD by heating the substrate from 5.5 K to 320 K at a rate of 0.5 K minutes $^{-1}$. Note that throughout the TPD process, the subliming molecules were detected via QMS (Extrel, Model 5221) operating in residual gas analyzer (RGA) mode operating, with electron impact ionizer of 100 eV, an emission current of 1 mA, and a mass range up to 500 amu.

To detect the subliming molecules with the isomer-selective PI-ReTOF-MS approach, the neutral molecules subliming in the TPD are ionized by pulsed VUV laser light close to 2 mm in front of the ice sample. The ions produced are mass-resolved and detected by a multichannel plate in a dual chevron configuration and then amplified by a fast preamplifier (Ortec 9305) and shaped with a 100 MHz discriminator. Finally, the spectra are recorded using a personal-computer-based multichannel scaler (FAST ComTec, P7888-1E) with 4 ns bin widths triggered at 30 Hz using a pulse delay generator (Quantum Composer, 9518) and 3600 sweeps per mass spectrum per 1 K increase in temperature during TPD. The experiments were taken out at different photoionization energies and additionally with $C^{18}O$ (Sigma Aldrich; 95% ^{18}O , 99.9% ^{12}C) to verify the composition of a desorbing molecule via isotopic mass shift.

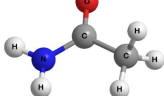
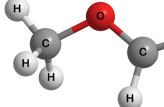
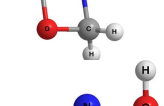
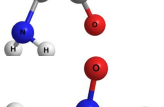
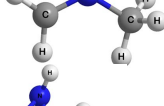
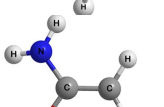
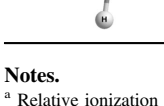
The VUV light is generated by difference-frequency mixing ($2\omega_1 - \omega_2$) in a noble gas (krypton (Kr)) using two dye lasers

(Sirah Lasertechnik, Model Cobra-Stretch, and Precision Scan) each pumped by a Nd:YAG laser (Spectra-Physics, Models PRO-270-30). In order to record and monitor the VUV light, a detection system consisting of a Faraday cup and a diode calibrated by the National Institute of Standards and Technology (NIST) is placed behind the detection region. This tunable VUV photon source allows soft-ionization of molecules with ideally no fragmentation (Förstel et al. 2015, 2016a, 2016d; Abplanalp & Kaiser 2017; Göbi et al. 2017). In this work we used a mixture of rhodamine 610 and rhodamine 640 in the first dye laser, pumped by 532 nm, to generate 606.948 nm, which is frequency-tripled to $\omega_1 = 202.316$ nm for the two-photon resonance of krypton (Kr). Adding the second dye laser with LDS 967 pumped by 532 nm with an output wavelength of $\omega_2 = 863$ nm, results in the VUV energy of 10.82 eV (114.6 nm). For the second VUV energy of 9.78 eV, the second dye laser with Coumarin 503 as dye is pumped by 355 nm to achieve $\omega_1 = 500$ nm (Table 2). Note that calibration data for the ReTOF reveal a lowering of the ionization energies of the subliming molecules by up to 0.03 to 0.04 eV due to the static electric field-induced Stark shift (Jones & Kaiser 2013).

3. Theoretical

The hybrid density functional B3LYP (Lee et al. 1988; Becke 1992a, 1992b, 1993) is exploited with the cc-pVTZ basis set to calculate the geometry of the neutral molecules and cations with the lowest energy. Afterwards, their coupled cluster, (Purvis & Bartlett 1982; Hampel et al. 1992; Knowles et al. 1993; Deegan & Knowles 1994) CCSD(T)/cc-pVDZ, CCSD(T)/cc-pVTZ, and CCSD(T)/cc-pVQZ, energies were calculated and extrapolated to completed basis set limits (Peterson et al. 1994) CCSD(T)/CBS, with B3LYP/cc-pVTZ zero-point energy corrections. Subsequently, the difference between the ionic and neutral states results in the adiabatic ionization energy of the respective isomer. The GAUSSIAN09 program (Frisch 2013) was utilized in the electronic structure calculations. Table 3 presents the calculated adiabatic ionization energies for the isomers of C_2NH_5O , along with the relative energies of the structural isomers considered in this study and ionization energy values from the literature. A comparison with the literature data of known ionization energies with theoretical values suggests that the calculations typically overestimate the ionization energies by 0.03 eV to

Table 3
Calculated Adiabatic Ionization Energies (IE) and Relative Energies (E_{rel}) of Distinct $\text{C}_2\text{NH}_5\text{O}$ Isomers

Structure	Molecular Formula	Species	IE, ^a eV	E_{rel} , ^b eV	Literature Value IE, eV
	<chem>HCONHCH3</chem>	<i>N</i> -methyl formamide	9.80	0.55	9.86 ^c
	<chem>NH2C(O)CH3</chem>	Acetamide	9.74	0.00	9.77 ^d
	<chem>CH3OCHNH</chem>	Methanimidic acid	9.71	1.35	
	<chem>OHC(NH)CH3</chem>	Ethanimidic acid	9.65	0.63	
	<chem>CH2NOCH3</chem>	O-methyl formaldoxime	9.51	2.83	
	<chem>NHCHCH2OH</chem>	2-imino ethanol	9.51	1.47	
	<chem>c-(CH2OCH2NH)</chem>	1,3-Oxazetidine	9.43	3.05	
	<chem>CH2NCH2OH</chem>	Methylene amino methanol	9.18	1.71	
	<chem>NH2CH2COH</chem>	Amino acetaldehyde	9.12	1.07	
	<chem>CH2N(O)CH3</chem>	<i>N</i> -methylene methanamine	9.02	2.95	
	<chem>c-(NHOCH)CH3</chem>	3-methyl oxaziridine	9.02	2.31	
	<chem>CH2CHONH2</chem>	O-ethenyl hydroxylamine	8.79	3.08	
	<chem>NH2C(CH2)OH</chem>	1-Amino ethenol	7.88	1.03	
	<chem>OHCHCHNH2</chem>	2-Amino ethenol	7.39	1.52	

Notes.

^a Relative ionization potential by CCSD(T)/CBS, with a B3LYP/cc-pVTZ zero-point energy correction in eV.

^b Relative energy by CCSD(T)/CBS, with a B3LYP/cc-pVTZ zero-point energy correction in eV.

^c Kimura et al. (1981).

^d Watanabe et al. (1962).

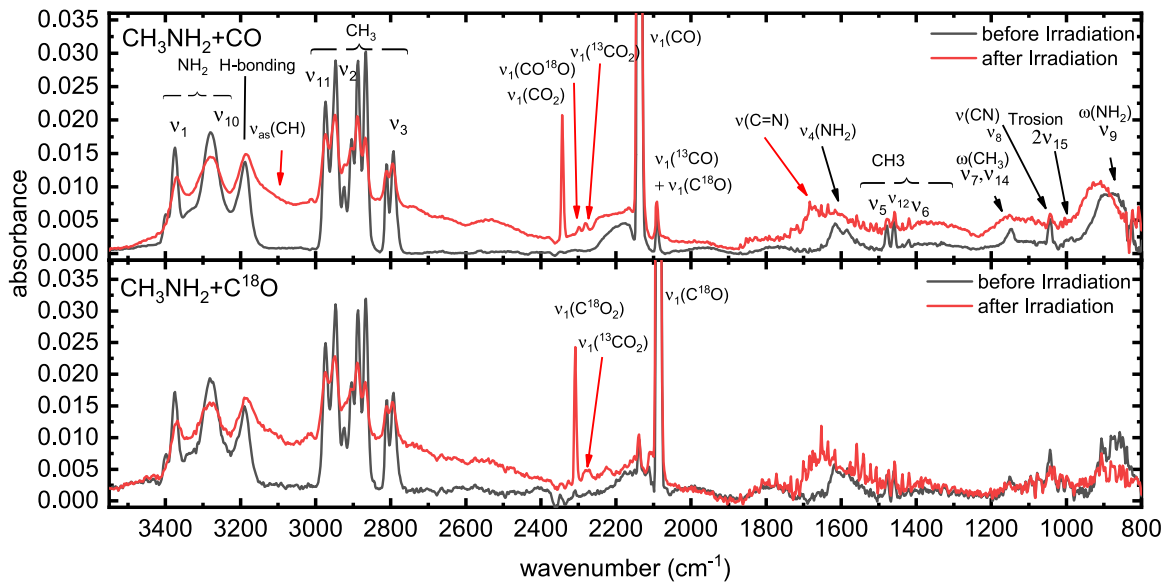


Figure 1. FTIR spectra before (black) and after (red) the irradiation of ice mixtures containing methylamine (CH_3NH_2) and carbon monoxide (CO) or its isotope (C^{18}O).

0.05 eV (Kaiser et al. 2010a, 2010b; Kostko et al. 2010; Kaiser et al. 2012).

4. Results

The infrared spectra recorded prior to the radiation exposure reveal characteristic absorption features of methylamine (CH_3NH_2) (Bossa et al. 2012) and carbon monoxide (CO) (Bennett et al. 2009, 2010) (Figure 1; Table 4). While the fundamental of carbon monoxide at 2136 cm^{-1} (CO-stretching, $\nu_1(\text{CO})$) along with the 2091 cm^{-1} (^{13}CO -stretching, $\nu_1(^{13}\text{CO})$) and 4251 cm^{-1} features (overtone $\nu_1(\text{CO})$) are clearly separated, the methylamine modes are overlapping. Three overlapping vibrations at 3332 cm^{-1} , 3260 cm^{-1} , and 3191 cm^{-1} are attributed to the antisymmetric (ν_{10}), symmetric (ν_1) NH_2 stretching and the hydrogen bonding between the molecules in the methylamine ice, respectively. The region of $3000\text{--}2700\text{ cm}^{-1}$ connects to two degenerate (ν_{11} , ν_2) and the symmetrical (ν_3) CH_3 stretching modes of methylamine. Their satellite peaks and peak shift are characteristic for Fermi resonances. Further absorption features are the NH_2 scissor mode (ν_4 , 1651 cm^{-1}), and the degenerate (ν_{12} , 1500 cm^{-1} , ν_5 , 1467 cm^{-1}) and symmetric (ν_6 , 1441 cm^{-1}) CH_3 deformations, followed by the CH_3 rocking (ν_7 , ν_{14} , 1182 cm^{-1}) modes, the C-N (ν_8 , 1049 cm^{-1}) stretching, the first overtone of the torsion (ν_{15} , 1005 cm^{-1}), and the NH_2 wagging modes (ν_9 , 955 cm^{-1}).

After the irradiation, several new absorption features emerged. These are attributed to products forming pure methylamine (CH_3NH_2) (Bossa et al. 2012) and carbon monoxide (CO) (Gerakines et al. 2005; Öberg et al. 2007; Bennett et al. 2009, 2010; Caro et al. 2010; Chen et al. 2014) ices upon irradiation. Features at 2343 cm^{-1} , 2300 cm^{-1} , and 2280 cm^{-1} result from stretching modes of the carbon dioxide (CO_2), along with its isotopically labelled counterparts $^{13}\text{CO}_2$ and CO^{18}O . Further absorptions at 1635 cm^{-1} and 3144 cm^{-1} originate from the C = N and the CH stretching of methanimine (CH_2NH) (Theule et al. 2011)—a product of methylamine (CH_3NH_2) dehydrogenation. Further absorptions are rather weak and based on the group frequencies most likely originate from amines (2380 cm^{-1} , 2165 cm^{-1}) (Socrates 2001)

Table 4
Infrared Adsorption Features of Methylamine, Its Irradiation Product Methanimine, and Carbon Monoxide with Its Irradiation Products; The Wavenumbers from Durig et al. (1968) for Methylamine, from Theule et al. (2011) for Methanimine, and from Jamieson et al. (2007) for CO and Its Irradiation Products

Wavenumber/ cm^{-1}	Vibration Mode	Assignment
CH_3NH_2		
3332	NH_2 antisymmetric stretching	ν_{10}
3260	NH_2 symmetric stretching	ν_1
3191	H bonding	
2942	CH_3 degenerate stretching	ν_{11}
2881	CH_3 degenerate stretching	ν_2
2793	CH_3 symmetric stretching	ν_3
1651	NH_2 scissors	ν_4
1500	CH_3 degenerate deformation	ν_{12}
1467	CH_3 degenerate deformation	ν_5
1441	CH_3 symmetric deformation	ν_6
1353	NH_2 twisting	ν_{13}
1182	CH_3 rocking	ν_7, ν_{14}
1048	CN stretching	ν_8
1005	Torsion first overtone	ν_{15}
955	NH_2 wagging	ν_9
processed CH_3NH_2		
3144	CH antisymmetric stretching	ν_a
1662	C = N stretching	$\nu(\text{C} = \text{N})$
CO		
4251	CO-stretching first overtone	ν_1
2208	CO-stretching + lattice vibration	$\nu_1 + \nu_L$
2136	CO-stretching	ν_1
2091	^{13}CO -stretching	$\nu_1(^{13}\text{CO})$
2088	C^{18}O stretching	$\nu_1(\text{C}^{18}\text{O})$
processed CO		
2342	CO_2	
2300	C^{18}OO	
2280	$^{13}\text{CO}_2$	

and alkanes (3009 cm^{-1}), (Socrates 2001) which could be associated with *N*-methyl formamide as well. The main feature of *N*-methyl formamide is expected around 1700 cm^{-1} , but due to the C=N-vibration of methanimine feature around

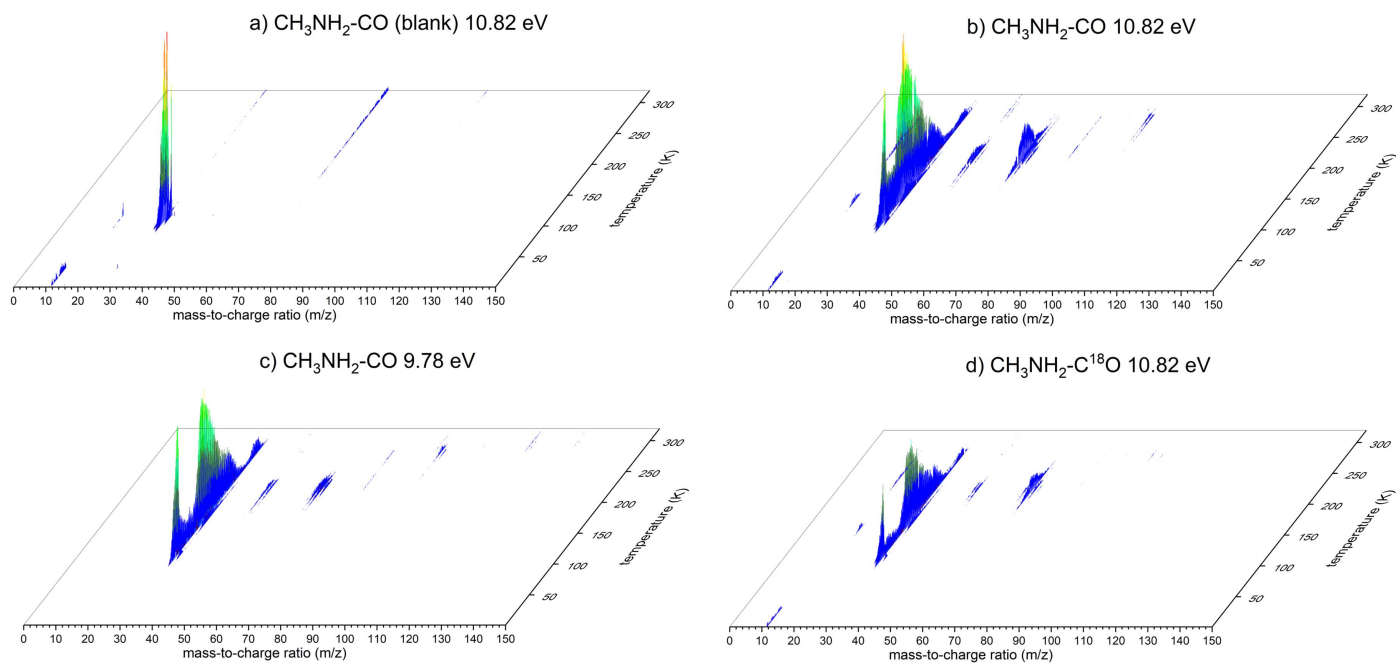


Figure 2. PI-ReTOF-MS spectra of the subliming molecules recorded at distinct ionization energies for the irradiated ice mixtures containing methylamine (CH_3NH_2) and carbon monoxide (CO) or its ^{18}O substituted counterpart (C^{18}O). Panel (a) shows the non-irradiated ice mixture ($\text{CH}_3\text{NH}_2\text{:CO}$) (blank).

1750 cm^{-1} and the NH_2 scissor feature at 1651 cm^{-1} , we cannot attribute any further features in this region. Taking into account the energy loss of the electrons while penetrating the ices (Table 1), we can calculate the parent molecules that are processed per eV. The differences between the integrated FTIR features before and after irradiation of the parent molecules result in $(1.0 \pm 0.3) \times 10^{17}$ methylamine (CH_3NH_2) and $(9.0 \pm 3.0) \times 10^{16}$ carbon monoxide (CO) molecules being destroyed during the irradiation. Since both carbon monoxide (CO) and methylamine (CH_3NH_2) are essential for the synthesis of *N*-methyl formamide (HCONHCH_3), we can determine the maximum conversion yield. If each destroyed pair of methylamine (CH_3NH_2) and carbon monoxide (CO) is converted to *N*-methyl formamide, upper yields of 0.03 ± 0.01 molecules eV^{-1} are extracted. Considering that $(2 \pm 1) \times 10^{15}$ carbon monoxide are also converted to carbon dioxide upon radiolysis, (Jones et al. 2011) these carbon monoxide molecules cannot be used in the synthesis of *N*-methyl formamide, thus reducing the yield to 0.024 ± 0.005 molecules eV^{-1} .

In order to gain a more detailed understanding on the products synthesized, PI-ReTOF-MS is exploited. Compared to FTIR, this approach is significantly more sensitive by up to 12 orders of magnitude and can discriminate between structural isomers (Abplanalp et al. 2016a; Zhu et al. 2018). The PI-ReTOF-MS data are compiled in Figure 2 for distinct ice mixtures and photon energies. Figures 2(a)/(b) show the PI-ReTOF-MS data of the unirradiated (blank) and irradiated ice mixtures, respectively, at the highest recorded photon energy of 10.82 eV. The blank experiment shows intense ion counts at mass-to-charge ratios (m/z) of 30, 31, and 32 in the temperature range of 90 to 120 K, which can be attributed to the parent molecule methylamine (CH_3NH_2), its isotope along with protonated methylamine $^{13}\text{CH}_3\text{NH}_2/\text{CH}_3\text{NH}_3^+$, plus the protonated version of the ^{13}C -methylamine $^{13}\text{CH}_3\text{NH}_3^+$. For the irradiated sample (Figure 2(b)) critical

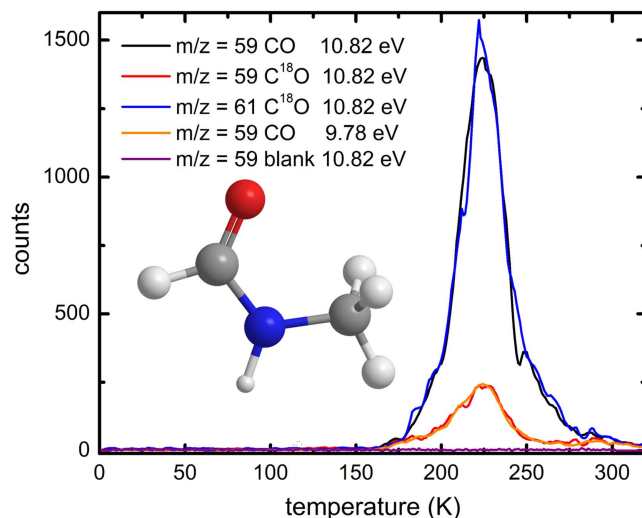


Figure 3. TPD profiles recorded at various mass-to-charge ratios and photon energies required for the detection of *N*-methyl formamide. The m/z ratios and photon energy of each trace are defined in the legend.

ion traces related to newly formed molecules are visible. Most importantly, a strong signal can be found between 175 K and 275 K at $m/z = 59$ ($\text{C}_2\text{H}_5\text{NO}^+$) (Figure 3)—the molecular parent ion originating from ionization of neutral *N*-methyl formamide and/or its isomers subliming into the gas phase, which is absent in the blank experiment. Therefore, we can conclude that the new signal $m/z = 59$ ($\text{C}_2\text{H}_5\text{NO}^+$) is directly linked to the radiation exposure of the methylamine–carbon monoxide ice to energetic electrons. Upon labeling the oxygen and irradiating $\text{CH}_3\text{NH}_2\text{-C}^{18}\text{O}$ ices, an essential identical TPD profile recorded at 10.82 eV photon energy shifts from $m/z = 59$ by 2 amu to $m/z = 61$ ($\text{C}_2\text{H}_5\text{N}^{18}\text{O}^+$), demonstrating that a single oxygen atom is in the newly formed molecule. It should be noted that in the

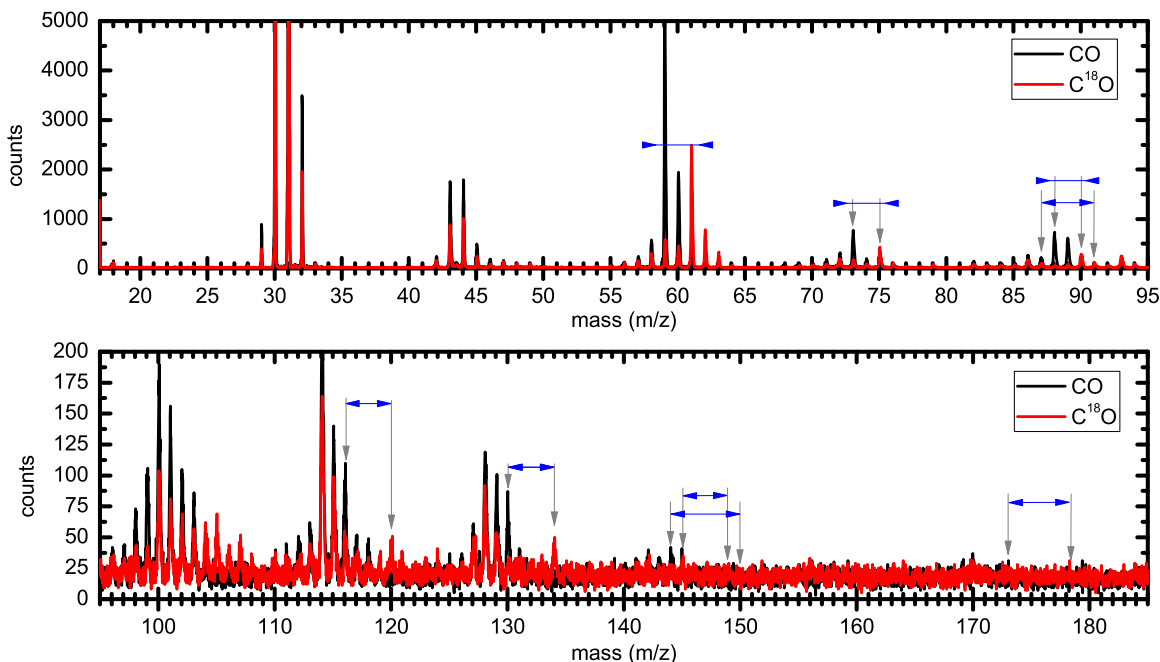


Figure 4. Photoionization mass spectrum integrated over the temperature from 5 K to 300 K for an ice mixture of methylamine (CH_3NH_2), with carbon monoxide (CO) and its ^{18}O substituted counterpart (C^{18}O).

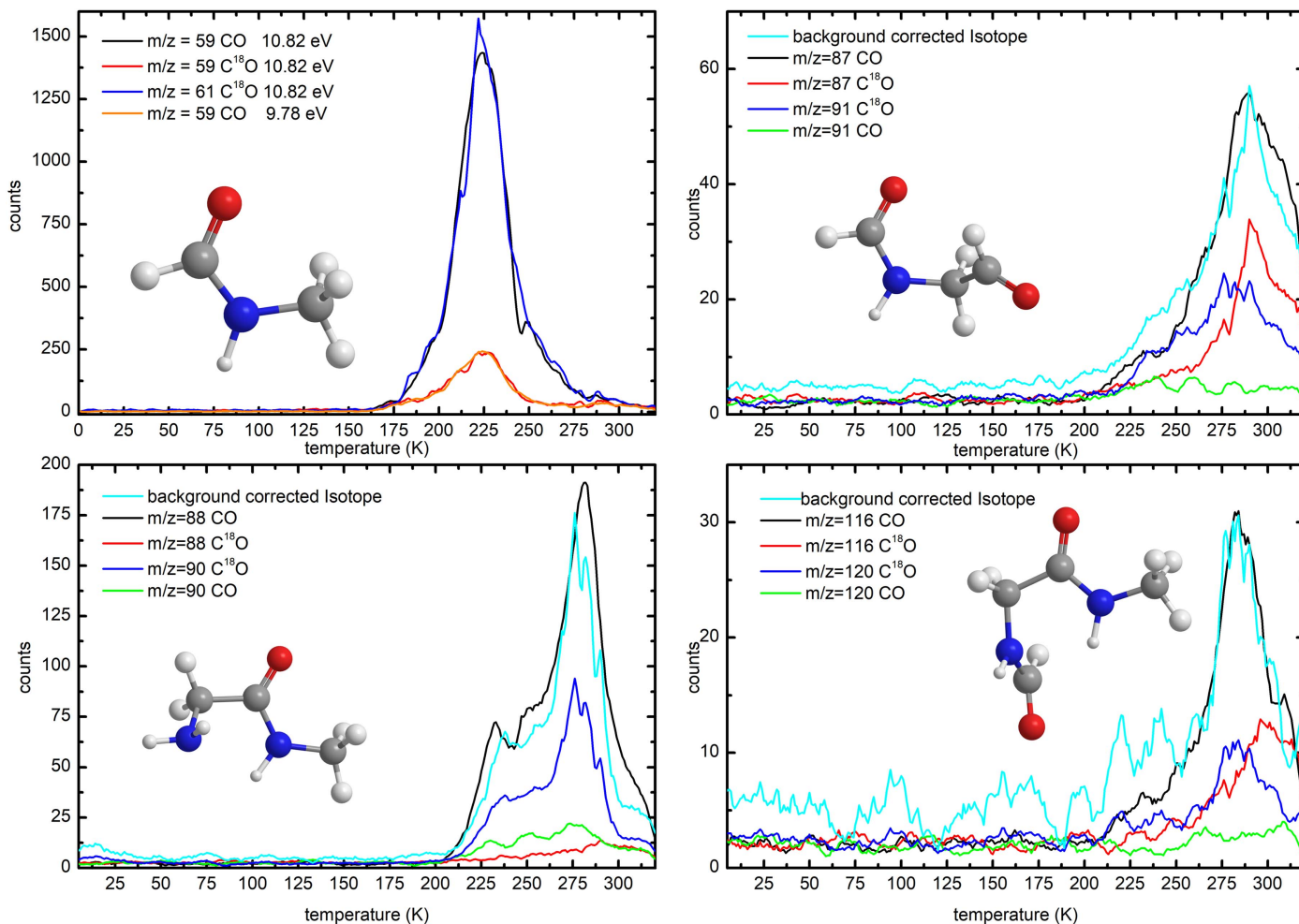


Figure 5. TPD profiles of *N*-methyl formamide, along with potential mass growth products formally carrying two *N*-methyl formamide units. The m/z ratios and carbon monoxide isotope present in the ice mixture used for each trace are given in the legend.

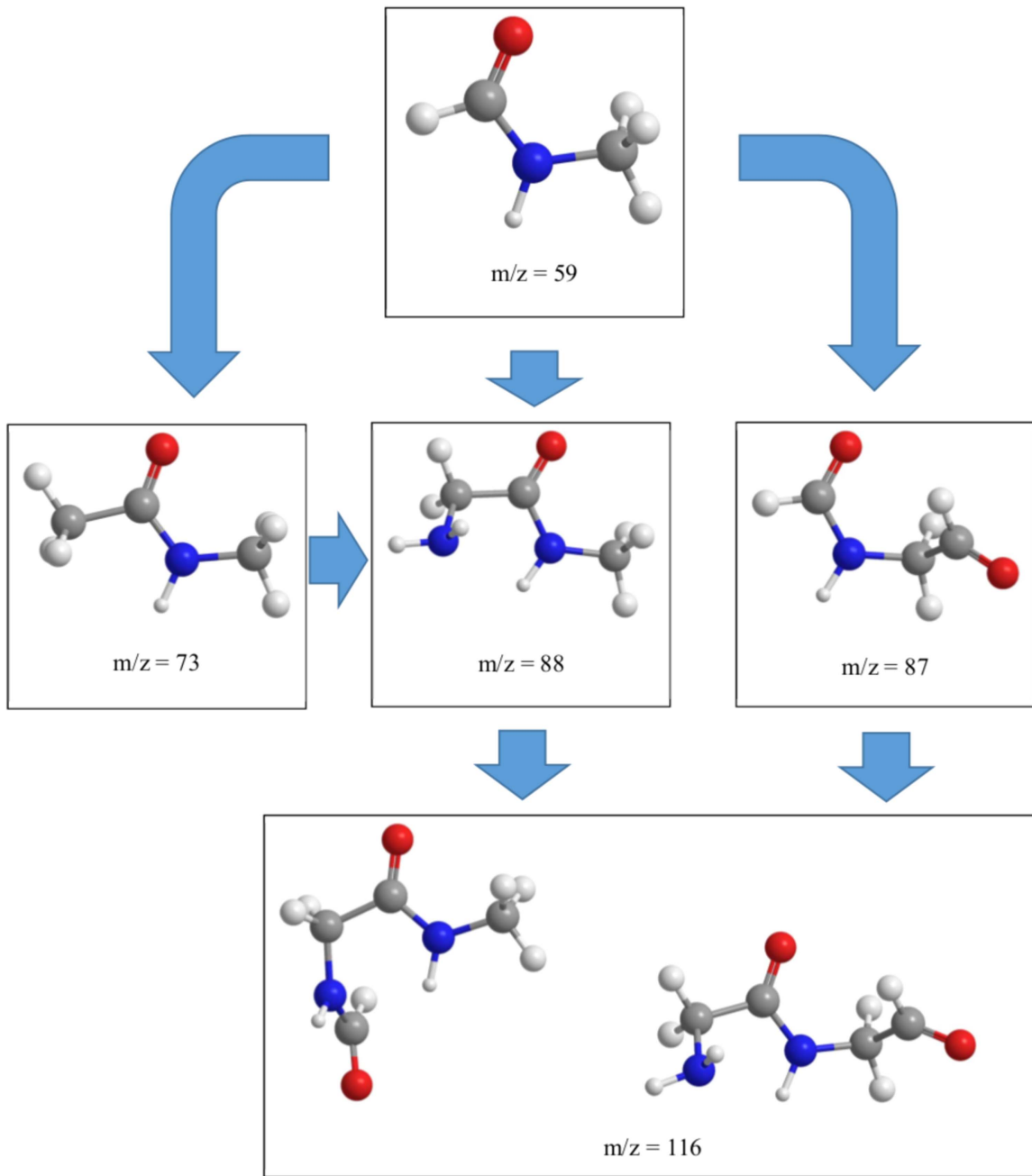


Figure 6. Possible mass growth processes, starting with *N*-methyl formamide formally carrying two *N*-methyl formamide units.

$\text{CH}_3\text{NH}_2\text{-C}^{18}\text{O}$ ices, low ion counts are still detectable at $m/z = 59$, whose TPD profile is different than the one recorded at $m/z = 61$. Naturally, the signal at $m/z = 59$ cannot originate from $\text{C}_2\text{H}_5\text{N}^{18}\text{O}^+$ ions. Once we lower the photon energy, the nature of this signal becomes clear. Here, the molecular formula $\text{C}_2\text{H}_5\text{NO}$ resembles 14 structural isomers (Table 3). *N*-methyl formamide (HCONHCH_3) has the highest adiabatic ionization energy of all isomers of 9.80 eV and 9.86 eV for the calculated and experimental values, respectively. Therefore, tuning the photon energy to 9.78 eV dictated that all $\text{C}_2\text{H}_5\text{NO}$ isomers except *N*-methyl formamide (HCONHCH_3) can be ionized. For the $\text{CH}_3\text{NH}_2\text{-CO}$ ices, the signal at $m/z = 59$ drops significantly; as a matter of fact, the TPD profile matches *exactly* the TPD profile of $m/z = 59$ recorded in the $\text{CH}_3\text{NH}_2\text{-C}^{18}\text{O}$

experiments. Therefore, the remaining ions contributing to the signal at $m/z = 59$ at 9.78 eV *cannot* have any oxygen atoms, but only carbon, nitrogen, and hydrogen. This in turn reveals that the signal at $m/z = 59$ and $m/z = 61$ obtained from the subliming $\text{CH}_3\text{NH}_2\text{-CO}$ and $\text{CH}_3\text{NH}_2\text{-C}^{18}\text{O}$ ices only originates from *N*-methyl formamide, along with its ^{18}O substituted counterpart, but not from any other $\text{C}_2\text{H}_5\text{NO}$ isomer. The previous experiment from Bossa et al. (2012) used the UV flux of 10^{15} photons $\text{s}^{-1} \text{cm}^{-2}$. This flux converts to about $14 \text{ eV molecule}^{-1}$ (Mason et al. 2014), which is in the same region as the energy dose used in this work. Their findings, however, only suggest the existence of *N*-methyl formamide, based on the QMS data. An isotope study or an analysis of the isomer structure of $m/z = 59$ as we present it in this study was not done in their study.

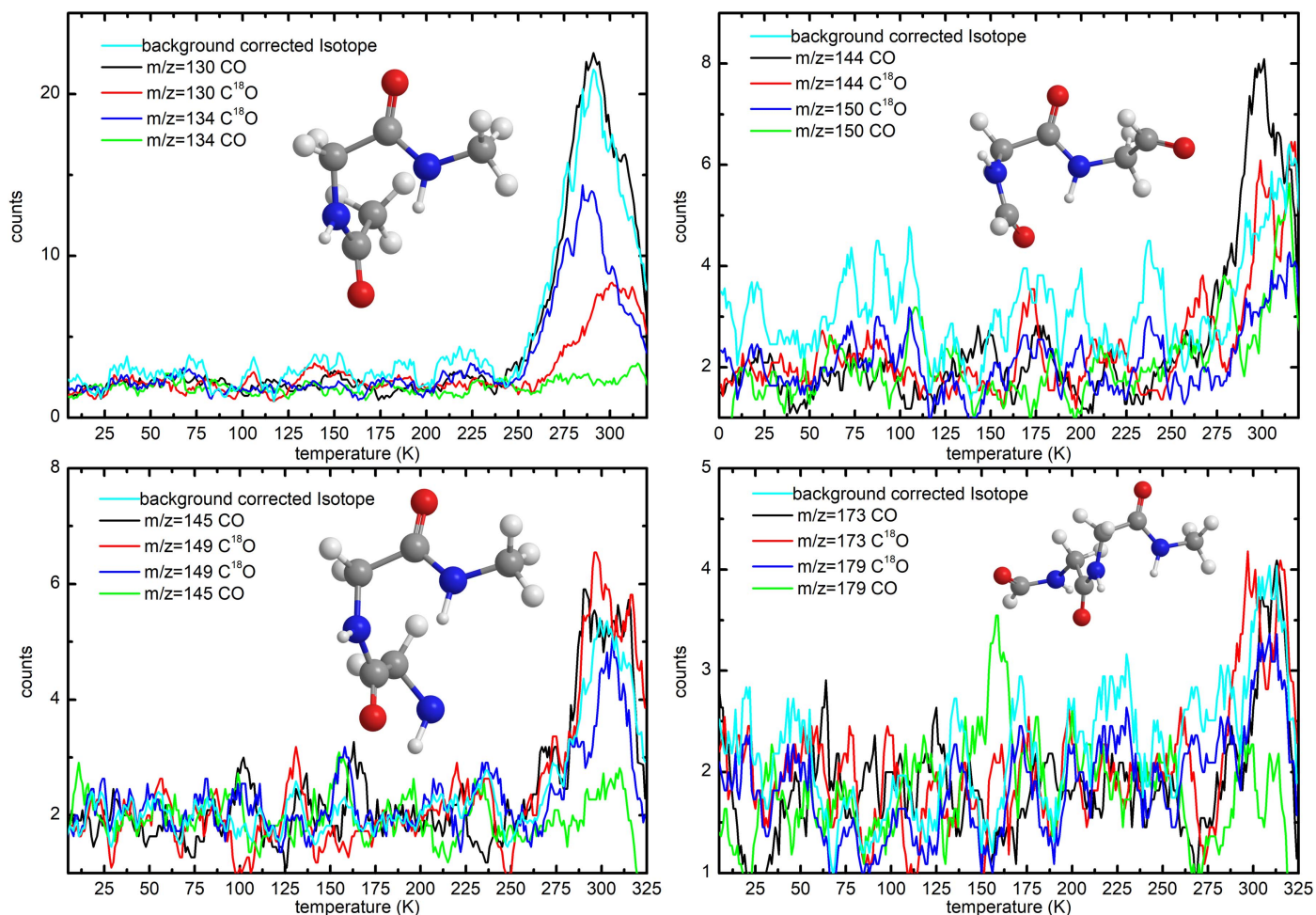
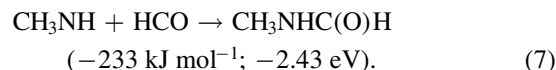
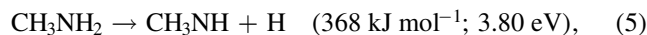
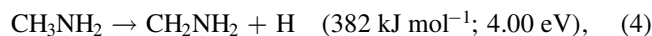


Figure 7. TPD profiles of possible mass growth processes leading to complex organics, with peptide bonds formally carrying three *N*-methyl formamide units.

5. Discussion

Having established the synthesis of *N*-methyl formamide (HCONHCH₃) upon interaction of energetic electrons with methylamine–carbon monoxide ices, we are now discussing possible formation routes. First, the *overall* reaction to synthesize *N*-methyl formamide from the reactants is endoergic by 0.79 eV (Equation (3)). These energetics alone dictate that the synthesis of *N*-methyl formamide *cannot* occur under thermal conditions below 10 K or during the warm-up phase. Therefore, non-equilibrium processes must be involved with the required energy supplied from the energetic electrons or—in real astrophysical environments—an external energy source such as that supplied by GCRs (Abplanalp et al. 2016a). Alternatively, experiments in the methylamine–carbon dioxide system exposed to energetic electrons (Holtom et al. 2005) revealed that methylamine can undergo unimolecular decomposition via atomic hydrogen loss either from the methyl group (CH₃) or from the amino group (NH₂) via reactions (4) and (5), respectively. These processes require that up to 3.80 eV be supplied by the impinging electrons and generate suprathermal hydrogen atoms holding kinetic energies of a few eV. This energy is sufficient to overcome the barrier to the addition of atomic hydrogen to the carbon–oxygen triple bond of carbon monoxide of 0.73 eV (70.7 kJ mol⁻¹) forming the formyl radical (HCO) through Equation (5) (Bennett et al. 2005; Bennett & Kaiser 2007; Kaiser et al. 2014; Maity et al.

2014, 2015; Maksyutenko et al. 2015). If both the formyl radical (HCO) and the methylamidogen radical (CH₃NH) are within the matrix cage and hold favorable geometries, they can recombine barrierlessly to *N*-methyl formamide (HCONHCH₃) (reaction (7)). Note that this reaction sequence mirrors the formation of acetaldehyde (CH₃CHO) and formamide (HCONH₂).



We would like to point out that the subliming molecules were also analyzed for methyl isocyanate (CH₃NCO, *m/z* = 57), which could represent a potential precursor to *N*-methyl formamide via hydrogenation. Although we found evidence for molecules formed with *m/z* = 57, the ¹⁸O labeled ices did not shift this profile to *m/z* = 59. Therefore, we can conclude that methyl isocyanate (CH₃NCO) is not formed in the present experiments, and thus *N*-methyl formamide cannot result from reduction of this species.

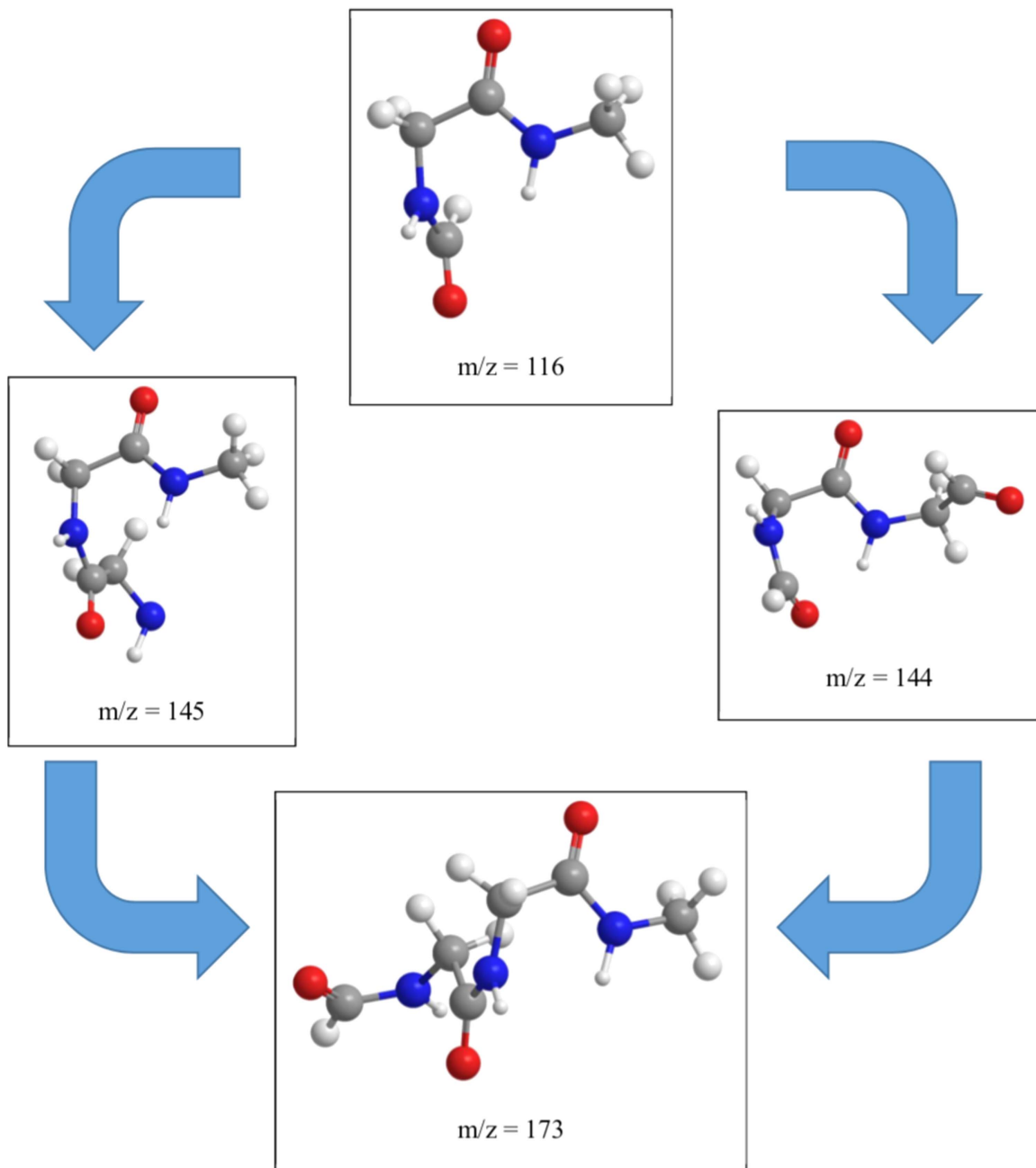


Figure 8. Possible mass growth processes leading to complex organics, with peptide bonds formally carrying three *N*-methyl formamide units.

Besides *N*-methyl formamide (HCONHCH_3 , $m/z = 59$), the signal at $m/z = 73$ depicts a strong isotopic shift, followed by ions at $m/z = 87$, 88 , and 116 . Considering the parent molecules and the significant amount of *N*-methyl formamide (HCONHCH_3) formed, the masses correlate with multiple building blocks of CH_2NH (29 amu) and CO (28 amu) units. The blue arrows in Figure 4 indicate the isotope shift, whereas Figure 5 presents the TPD traces for the designated ions and their isotopic counterparts for both ice mixtures. While the TPD traces (black and blue curves, Figure 5) extracted from the subliming molecules of both ice mixtures obviously overlap for *N*-methyl formamide (HCONHCH_3 , $m/z = 59$ and $m/z = 61$), for higher mass-to-charge ratios, interference from molecules with identical mass-to-charge ratios but without oxygen (O) are obscuring a direct comparison. This signal is presented in green

and red in Figure 5. Therefore, a background correction has to be introduced. In this work, we subtract the background signal at the higher m/z (green curve) from the signal connected with the isotopically substituted trace (dark blue curve) and add the background signal of the low m/z trace (red curve). The result is presented in Figure 5 as a light blue curve. Starting from *N*-methyl formamide (HCONHCH_3), $m/z = 87$ most likely results from incorporation of a single carbon monoxide (CO) unit, while $m/z = 88$ could originate from CH_2NH_2 incorporation to *N*-methyl formamide (HCONHCH_3). This is supported by the isotopic shifts by 4 amu and 2 amu for $m/z = 87$ and $m/z = 88$, respectively. A mass-to-charge ratio of 116 can be achieved formally via the recombination of two *N*-methyl formamide (HCONHCH_3) molecules or successive incorporation of carbon monoxide (CO) and the CH_2NH_2 building block,

as presented in Figure 6. The insets in Figure 5 show the molecular structures that suggest peptide polymerization in the ice mixtures as presented in Figure 6. Further isotopic shifts presented in Figure 4 for $m/z = 130, 144, 145,$ and 173 are plotted in Figure 7 in the same pattern as in Figure 5. Although the signals are very small, the isotopically shifted traces can still be overlapped. Possible molecular structures are presented in Figure 8. These findings allow speculation about the formation and presence of peptide bonds toward organic molecules in astrophysically relevant ices. Förstel et al. (2016b) reported the results of polyamide formation in irradiated ice mixtures of carbon monoxide (CO) with ammonia (NH₃). Furthermore, Halfen et al. (2011) predicted an abiotic formation for polypeptide under interstellar conditions similar to the present study. However, since several isomers for each mass-to-charge ratio exist, without the knowledge of the ionization energies, these results can only be regarded as tentative and have to be confirmed in future studies.

6. Conclusion

In this study, we elucidated the formation of *N*-methyl formamide (HCONHCH₃) in astrophysical model ices of methylamine (CH₃NH₂) and carbon monoxide (CO), upon irradiation with energetic electrons as generated in the track of galactic cosmic ray particles (GCRs) penetrating interstellar ices as present on ice-coated nanoparticles in cold molecular clouds such as the Taurus Molecular Cloud 1 (TMC-1) at typical temperatures of 10 K. The synthesis is governed by an initial decomposition of methylamine (CH₃NH₂) to the methylamidogen radical (CH₃NH), along with suprathreshold hydrogen atoms, which in turn can overcome the barrier of addition to the carbon monoxide molecule leading to the formyl radical (HCO). Within the matrix cage, both the formyl and methylamidogen radical may recombine barrierlessly to form the *N*-methyl formamide molecule. Once the molecular cloud transforms to star-forming regions, the newly formed molecules sublime from the ices as the temperature of the grains rises due to the non-isothermal phase of collapse and later due to heating from the hot core. Eventually, the processed matter enters the circumstellar disk and is incorporated at least partially into planetary bodies (planets, moons, comets), thus providing the raw material for stellar systems, including our own. As one of the simplest molecules containing a peptide bond (–CO–NH–), *N*-methyl formamide could represent a key molecule involved in radiation-induced peptide bond polymerization in extraterrestrial ices.

Although *N*-methyl formamide is only tentatively observed in the star-forming region Sgr B2(N2), (Belloche et al. 2017), our results support the detection of *N*-methyl formamide. Considering the complex rotational spectrum of *N*-methyl formamide due to a strong torsion-rotation interaction, searching for *N*-methyl formamide in extraterrestrial environments is a challenging task. In contrast, the rotational spectra of the related formamide (HCONH₂) and acetamide (CH₃CONH₂)—an isomer of *N*-methyl formamide—are relatively “simple,” and hence both molecules were already observed in 1971 (Rubin et al. 1971) and 2006 (Hollis et al. 2006), respectively, toward Sgr B2(N2). The lack of detection of acetamide (CH₃CONH₂) in our studies can be rationalized by the necessity of generating reactive methyl (CH₃) and amidogen (NH₂) radicals. However, the unimolecular decomposition of the methylamine precursor (CH₃NH₂) could lead, in principle, to carbon–nitrogen rupture to these radicals in

the gas phase, (Michael & Noyes 1963) but not in the condensed phase (Holtom et al. 2005), where the matrix cage facilitates recycling of the methylamine molecule via radical–radical reaction of methyl with amidogen.

As molecules synthesized in small yields become more complex, infrared spectra and in particular the group frequencies of the products significantly overlap and cannot be distinguished from each other. This is especially the case for molecules that have infrared active functional groups in common, such as the carbonyl group (C=O) and the peptide bond (–CO–NH–). Therefore, alternative techniques are imperative to advancing the field, such as the PI-ReTOF-MS as exploited here. This approach has the unique capability to detect individual molecules based on their ionization energies, even in the complex mixtures produced during the exposure of astrophysical model ices to ionizing radiation. With the commission of the Atacama Large Millimeter/Submillimeter Array (ALMA), more complex (biorelevant) organic molecules will be identified. Understanding these data will require advances in experimental laboratory astrophysics. Ultimately, further insight into the link between the origin and evolution of comets and the interstellar material that created them will bring us closer to revealing where in the Universe the molecular precursors linked to the origins of life might have been synthesized.

Even though *N*-methyl formamide (HCONHCH₃) represents the predominant molecule formed in the present experiment, Figure 2 alone reveals evidence for molecules with higher mass-to-charge ratios. Furthermore, the temperature-integrated mass-to-charge spectrum in Figure 4 presents mass-to-charge ratios of up to 180, for both ice mixtures with carbon monoxide (CO, Figure 4, black curve) and with its isotope (C¹⁸O, Figure 4, red curve), respectively. While comparing the two ice mixtures, the differences indicate isotopic shifts of products containing oxygen (O) atoms, i.e., by 2 amu per oxygen atom.

The authors from Hawaii acknowledge support from the US National Science Foundation (AST-1505502). Furthermore, we thank the W. M. Keck Foundation for financing the experimental setup. The Taiwanese group (AHHC) thanks the National Center for High-performance Computing in Taiwan for providing the computer resources in the calculations.

ORCID iDs

Alexandre Bergantini  <https://orcid.org/0000-0003-2279-166X>

Ralf I. Kaiser  <https://orcid.org/0000-0002-7233-7206>

References

- Abplanalp, M. J., Förstel, M., & Kaiser, R. I. 2016a, *CPL*, **644**, 79
- Abplanalp, M. J., Gozem, S., Krylov, A. I., et al. 2016b, *PNAS*, **113**, 7727
- Abplanalp, M. J., & Kaiser, R. I. 2017, *ApJ*, **836**, 195
- Becke, A. D. 1992a, *JChPh*, **96**, 2155
- Becke, A. D. 1992b, *JChPh*, **97**, 9173
- Becke, A. D. 1993, *JChPh*, **98**, 5648
- Belloche, A., Meshcheryakov, A. A., Garrod, R. T., et al. 2017, *A&A*, **601**, A49
- Bennett, C. J., Chen, S.-H., Sun, B.-J., et al. 2007, *ApJ*, **660**, 1588
- Bennett, C. J., Jamieson, C. S., & Kaiser, R. I. 2009, *ApJS*, **182**, 1
- Bennett, C. J., Jamieson, C. S., & Kaiser, R. I. 2010, *PCCP*, **12**, 4032
- Bennett, C. J., Jamieson, C. S., Osamura, Y., & Kaiser, R. I. 2005, *ApJ*, **624**, 1097
- Bennett, C. J., & Kaiser, R. I. 2007, *ApJ*, **661**, 899
- Boogert, A. C. A., Schutte, W. A., Helmich, F. P., et al. 1997, *A&A*, **317**, 929

- Boogert, A. C. A., Schutte, W. A., Tielens, A. G. G. M., et al. 1996, *A&A*, **315**, L377
- Bossa, J.-B., Borget, F., Duvernay, F., et al. 2012, *AJCh*, **65**, 129
- Bouilloud, M., Fray, N., Bénilan, Y., et al. 2015, *MNRAS*, **451**, 2145
- Caro, G. M. M., Jiménez-Escobar, A., Martín-Gago, J. A., et al. 2010, *A&A*, **522**, A108
- Chen, Y.-J., Chuang, K.-J., Caro, G. M. M., et al. 2014, *ApJ*, **781**, 15
- Deegan, M. J. O., & Knowles, P. J. 1994, *CPL*, **227**, 321
- Drouin, D., Couture, A. R., Joly, D., et al. 2007, *Scanning*, **29**, 92
- Durig, J. R., Bush, S. F., & Baglin, F. G. 1968, *JChPh*, **49**, 2106
- Ehrenfreund, P., & Charnley, S. B. 2000, *ARA&A*, **38**, 427
- Ehrenfreund, P., Krafft, C., Kochan, H., & Pirronello, V. 2012, *Laboratory Astrophysics and Space Research*, Vol. 236 (Springer Science Business Media)
- Förstel, M., Bergantini, A., Maksyutenko, P., et al. 2017, *ApJ*, **845**, 83
- Förstel, M., Maksyutenko, P., Jones, B. M., et al. 2016a, *ChCom*, **52**, 741
- Förstel, M., Maksyutenko, P., Jones, B. M., et al. 2015, *Chem. Phys. Chem.*, **16**, 3139
- Förstel, M., Maksyutenko, P., Jones, B. M., et al. 2016b, *ApJ*, **820**, 117
- Förstel, M., Maksyutenko, P., Mebel, A. M., & Kaiser, R. I. 2016c, *ApJL*, **818**, L30
- Förstel, M., Tsegaw, Y. A., Maksyutenko, P., et al. 2016d, *Chem. Phys. Chem.*, **17**, 2726
- Fourikis, N., Takagi, K., & Morimoto, M. 1974, *ApJL*, **191**, L139
- Frisch, M. J. 2013, GAUSSIAN 09, Revision D01
- Garrod, R. T., Weaver, S. L. W., & Herbst, E. 2008, *ApJ*, **682**, 283
- Gerakines, P. A., Bray, J. J., Davis, A., & Richey, C. R. 2005, *ApJ*, **620**, 1140
- Góbi, S., Förstel, M., Maksyutenko, P., & Kaiser, R. I. 2017, *ApJ*, **835**, 241
- Gottlieb, C. A., Palmer, P., Rickard, L. J., & Zuckerman, B. 1973, *ApJ*, **182**, 699
- Gürtler, J., Klaas, U., Henning, T., et al. 2002, *A&A*, **390**, 1075
- Halfen, D. T., Ilyushin, V., & Ziurys, L. M. 2011, *ApJ*, **743**, 60
- Hampel, C., Peterson, K. A., & Werner, H.-J. 1992, *CPL*, **190**, 1
- Herbst, E., & van Dishoeck, E. F. 2009, *ARA&A*, **47**, 427
- Hollis, J. M., Lovas, F. J., Remijan, A. J., et al. 2006, *ApJL*, **643**, L25
- Holtom, P. D., Bennett, C. J., Osamura, Y., et al. 2005, *ApJ*, **626**, 940
- Holtom, P. D., Dawes, A., Davis, M. P., et al. 2007, *RaPC*, **76**, 745
- Jamieson, C. S., Mebel, A. M., & Kaiser, R. I. 2007, *CPL*, **443**, 49
- Jones, B. M., Bennett, C. J., & Kaiser, R. I. 2011, *ApJ*, **734**, 78
- Jones, B. M., & Kaiser, R. I. 2013, *J. Phys. Chem. Letters*, **4**, 1965
- Kaiser, R. I., Krishtal, S. P., Mebel, A. M., et al. 2012, *ApJ*, **761**, 178
- Kaiser, R. I., Maity, S., & Jones, B. M. 2014, *PCCP*, **16**, 3399
- Kaiser, R. I., Maity, S., & Jones, B. M. 2015, *Angew. Chem. Int. Ed.*, **54**, 195
- Kaiser, R. I., Maksyutenko, P., Ennis, C., et al. 2010a, *FaDi*, **147**, 429
- Kaiser, R. I., Stockton, A. M., Kim, Y. S., et al. 2013, *ApJ*, **765**, 111
- Kaiser, R. I., Sun, B. J., Lin, H. M., et al. 2010b, *ApJ*, **719**, 1884
- Kimura, K., Katsumata, S., Achiba, Y., et al. 1981, in *Handbook of HeI Photoelectron Spectra of Fundamental Organic Compounds* (New York: Halsted Press), 268
- Knowles, P. J., Hampel, C., & Werner, H. J. 1993, *JChPh*, **99**, 5219
- Kostko, O., Zhou, J., Sun, B. J., et al. 2010, *ApJ*, **717**, 674
- Lee, C., Yang, W., & Parr, R. G. 1988, *PhRvB*, **37**, 785
- Ligterink, N. F. W., Coutens, A., Kofman, V., et al. 2017, *MNRAS*, **469**, 2219
- Maity, S., Kaiser, R. I., & Jones, B. M. 2014, *FaDi*, **168**, 485
- Maity, S., Kaiser, R. I., & Jones, B. M. 2015, *PCCP*, **17**, 3081
- Maksyutenko, P., Muzangwa, L. G., Jones, B. M., & Kaiser, R. I. 2015, *PCCP*, **17**, 7514
- Malkov, A. V., Stončius, S., MacDougall, K. N., et al. 2006, *Tetrahedron*, **62**, 264
- Mason, N. J., Nair, B., Jheeta, S., & Szymańska, E. 2014, *FaDi*, **168**, 235
- Michael, J. V., & Noyes, W. A. 1963, *JChS*, **85**, 1228
- Moore, M. H., Hudson, R. L., & Gerakines, P. A. 2001, *AcSpA*, **57**, 843
- Öberg, K. I., Fuchs, G. W., Awad, Z., et al. 2007, *ApJL*, **662**, L23
- Peterson, K. A., Woon, D. E., & Dunning, T. H. 1994, *JChPh*, **100**, 7410
- Purvis, G. D., & Bartlett, R. J. 1982, *JChPh*, **76**, 1910
- Reach, W. T., Kelley, M. S., & Vaubailon, J. 2013, *Icar*, **226**, 777
- Rubin, R. H., Swenson, G. W., Benson, R. C., et al. 1971, *ApJL*, **169**, L39
- Socrates, G. 2001, *Infrared and Raman Characteristic Group Frequencies: Tables and Charts* (New York: Wiley)
- Tarczay, G., Förstel, M., Maksyutenko, P., & Kaiser, R. I. 2016, *InCh*, **55**, 8776
- Theule, P., Borget, F., Mispelaer, F., et al. 2011, *A&A*, **534**, A64
- Tsegaw, Y. A., Góbi, S., Förstel, M., et al. 2017, *JPCA*, **121**, 7477
- Turner, A. M., Abplanalp, M. J., Chen, S. Y., et al. 2015, *PCCP*, **17**, 27281
- Turner, A. M., Abplanalp, M. J., & Kaiser, R. I. 2016, *ApJ*, **819**, 97
- Walsh, C., Herbst, E., Nomura, H., et al. 2014, *FaDi*, **168**, 389
- Watanabe, K., Nakayama, T., & Mottl, J. 1962, *JQSRT*, **2**, 369
- Zhu, C., Turner, A. M., Abplanalp, M. J., & Kaiser, R. I. 2018, *ApJS*, **234**, 15